Oxidation of Platinum Nickel Nanowires to Improve Durability of Oxygen-Reducing Electrocatalysts

Shaun M. Alia,[a] Svitlana Pylypenko,[b,*] Arrelaine Dameron,[a] K. C. Neyerlin,[a] Shyam S. Kocha,[a,*] and Bryan S. Pivovar[a,*,z]

[a]*Chemical and Materials Science Center, National Renewable Energy Laboratory, Golden, Colorado 80401, USA*
[b]*Department of Chemistry, Colorado School of Mines, Golden, Colorado 80401, USA*

The impact of heat treating platinum-coated nickel (Pt-Ni) nanowires in oxygen is examined to determine the effect on oxygen reduction (ORR) activity and durability. Pt-Ni nanowires exhibit promising ORR mass activities (3 times greater than Pt nanoparticles, 1.5 times greater than U.S. Department of Energy target) both before and after potential cycling for all but the highest annealing temperatures explored. The annealing of Pt-Ni nanowires in oxygen with increasing temperature is found to reduce surface area and ORR activity in comparison to the untreated material, but also reduces activity losses following durability testing. Following potential cycling, unannealed Pt-Ni nanowires show significant losses in surface area (23%) and specific activity (18%) while Pt-Ni nanowires annealed at 200°C show modest increases in surface area (2%) and specific activity (6%) after potential cycling. Increasing annealing temperatures also show a clear trend of decreasing Ni dissolution rates. While oxygen annealing has shown the ability to improve durability of Pt-Ni nanowires, significant Ni dissolution was observed in all samples and suggests oxide passivation while showing promise for improved durability, when employed by itself is insufficient to prevent all contamination concerns involving Ni dissolution.

Manuscript submitted October 12, 2015; revised manuscript received December 31, 2015. Published January 12, 2016. This was Paper 1035 presented at the Cancun, Mexico, Meeting of the Society, October 5–9, 2014.

Platinum-nickel (Pt-Ni) nanowires are relatively recent additions to the family of advanced catalysts for fuel cell applications.[1] They have shown exceptionally high surface areas and mass activities and reasonable durability in rotating disk electrode (RDE) tests. Ni dissolution from these materials, however, is a concern in membrane electrode assemblies (MEAs) that doesn't necessarily impact RDE. This paper presents a study on the use of oxygen annealing to create more durable structures.

The commercial deployment of proton exchange membrane fuel cells (PEMFCs) has been limited by catalyst cost, performance, and durability. Platinum (Pt) nanoparticles supported on high surface area carbon (Pt/HSC) are typically used in PEMFCs due to a high Pt surface area and moderate mass activity in the oxygen reduction reaction (ORR). Further improvement in ORR mass activity is needed, however, to reach PEMFC cost targets and for PEMFCs to be more competitive commercially. Additionally, there are concerns for the durability of Pt/HSC when used in PEMFCs, where activity loss is commonly due to carbon corrosion and Pt surface area loss from Ostwald ripening, dissolution, and aggregation.[2,3]

The U.S. Department of Energy (DOE) set a 2020 out-year target of 440 mA mg^{-1} for ORR mass activity on a Pt group metal basis in transportation-based PEMFCs.[4] This target is intended for membrane electrode assemblies (MEAs), not activities in RDE. The catalysts in this manuscript are characterized in RDE half-cells, but occasionally compare the activities to the DOE-MEA target. RDE is typically used as a method for catalyst screening, requiring small sample sizes and less electrode optimization than commonly required in MEAs. RDE testing is a useful metric in evaluating catalyst activity, but is less prone than MEAs to activity losses (transport, resistance) and does not guarantee similar MEA performance.

Pt-Ni catalysts have previously been developed and studied for ORR activity. In polycrystalline films, Pt-Ni was found to have twice the site-specific activity of Pt.[5–7] Stamenkovic et al. further examined single facets, finding that alloying Pt (111) with Ni (Pt_3Ni) improved activity by an order of magnitude.[8] Additional studies have been completed on Pt-Ni nanoparticles, octahedra, and nanostructured thin films, each demonstrating improvements to conventional Pt catalysts.[9–19] In several cases, these materials have exceeded the DOE-MEA target in RDE half-cells.

Extended Pt surfaces are of interest in ORR since the catalyst type typically produces an order of magnitude higher site-specific activity. One example of extended surface catalysts is 3M, who previously developed nanostructured thin films for PEMFCs by depositing Pt, and Pt combined with other transition metals, onto organic whiskers.[20] Although extended surfaces generally produce high specific activities, their surface areas are traditionally low. Spontaneous galvanic displacement can be beneficial as a synthesis route since it allows for the deposition of thin Pt films and can produce higher surface areas.[1,21–26] Previously, Pt-Ni nanowires were developed with ORR mass activities 3 times greater than Pt/HSC and 1.5 times greater than the DOE-MEA target.[1] The high mass activity resulted from the high specific activity generally associated with extended surfaces, and electrochemical surface areas (ECAs) in excess of 90 $m^2\ g_{Pt}{}^{-1}$, a significant breakthrough for extended surface catalysts. Pt-cobalt (Co) nanowires were also examined previously and produced similar mass activities, but with lower ECAs and higher specific activities.[26]

The behavior of the Pt-Ni nanowires was found to be significantly different from the Pt-Co system in that the oxide layer resisted dissolution. This resistance appeared to contribute to the decreased extent of Pt displacement, perhaps enabling the synthesis of nanowires with high Pt ECAs. The study of Pt-Ni nanowires with low Pt displacement (7 wt% Pt) was chosen due to its high performance, but has elevated concerns for Ni dissolution due to the high Ni content. If Ni dissolution concerns can be overcome in these systems, the benefits of the extended surface and core shell approaches may be realized as enabling components of fuel cell systems.[27] The benefits of extended surfaces include the high activity associated with extended surface catalysts, long-term durability, and long-range conductivity of the metal Ni nanowire core, which provides electronic pathways independent of individual point contacts to carbon.

Experimental

Pt-Ni nanowires were synthesized by the partial galvanic displacement of Ni nanowires by previously reported methods.[1] Pt-Ni nanowires were annealed in oxygen (50% oxygen, 50% inert) for two

*Electrochemical Society Active Member.
[z]E-mail: bryan.pivovar@nrel.gov

hours (with a 10°C min^{-1} ramp rate) with a low flow rate and 500 torr of back pressure.

The dimensions, morphology and composition of Pt-Ni nanowires were determined by scanning electron microscopy (SEM) and energy dispersive X-ray spectroscopy (EDS) analysis performed on a JEOL JSM-7000F field emission microscope equipped with an EDAX Genesis energy dispersive X-ray spectrometer. Surface elemental composition and chemical states were examined using X-ray photoelectron spectroscopy (XPS), performed on a Kratos Nova X-ray photoelectron spectrometer equipped with a monochromatic Al Kά source operated at 300 W. During spectra acquisition, samples were subject to charge compensation using low energy electrons. Survey and high-resolution C 1s, O1s, Ni 2p and Pt 4f spectra were collected from three different areas on each sample using pass energies of 160 and 20 eV. Data processing was performed using CasaXPS software, employing sensitivity factors supplied by manufacturer. After subtraction of the linear (for C 1s and O1s) and Shirley (for Ni 2p and Pt 4f) backgrounds, spectra were charge-referenced to aliphatic carbon at 285.0 eV.

Inductively coupled plasma-mass spectrometry (ICP-MS) measurements were taken with a Thermo Scientific iCAP Q, calibrated to a blank and three Pt-Ni standards. Each unknown was measured three times at a dwell time of 0.15 s and with less than a 2% deviation between measurements. X-ray diffraction (XRD) patterns were taken using a Bruker D8 Discover, operating at 40 kV and 35 mA, with exposures of 60 min to a 2θ of 15–87°.

Electrochemical measurements were taken using a RDE half-cell with a glassy carbon working electrode, a Pt mesh counter electrode, and a reversible hydrogen electrode (RHE) reference in a 0.1 M perchloric acid electrolyte. Samples were weighed to make catalyst inks at concentrations of 0.2 mg_{PtNi} ml^{-1} and consisted of water and 2-propanol at a ratio of 3.8:1.2. Nafion ionomer was added to the ink at a concentration of 4 μl ml^{-1}. Three separate aliquots of the inks (100 μl) were dried and weighed on a microbalance to confirm ink concentration. Graphitized carbon nanofibers (Tanaka Kikinzoku Kogyo, Type 2) were added to the inks (60 wt%) to improve ink dispersion and the uniformity of electrode coating.[28] Inks were horn sonicated for 30 s, bath sonicated for 20 min, and horn sonicated for 30 s prior to pipetting 10 μl of ink onto a working electrode. The sonication process was repeated while the working electrodes dried (for 20 min in air at 40°C) in order to build the electrode loading (to 30.6 μg cm_{elec}^{-2}) to reach a proper diffusion limited current. Pt/HSC (46 wt% Pt, Tanaka Kikinzoku Kogyo) inks were made by combining 7.6 mg of catalyst with 7.6 ml of water, 2.4 ml of 2-propanol, and 40 μl of Nafion ionomer. After 20 min of bath sonication, 10 μl of ink were pipetted onto a working electrode, which was dried for 20 min in air at 40°C.

ECAs were determined by carbon monoxide oxidation and confirmed with hydrogen underpotential deposition. Carbon monoxide oxidation voltammograms were taken by holding the working electrode at 0.1 V vs. RHE for 20 min, the first 10 with carbon monoxide (Matheson Research Purity, 99.998%) and the second 10 with nitrogen bubbling into the electrolyte. Cyclic voltammograms were then immediately run at 20 mV s^{-1} starting at 0.1 V vs. RHE in the anodic direction. The first voltammogram was used to calculate ECAs, assuming a coulombic charge of 420 μC cm_{Pt}^{-2}. The subsequent voltammograms were used to confirm that no carbon monoxide persisted in the electrolyte following the adsorption period and served to validate the ECA calculation. ECAs by hydrogen underpotential deposition were determined from cyclic voltammograms at 20 mV s^{-1} in a nitrogen-saturated 0.1 M perchloric acid electrolyte and were calculated assuming a coulombic charge of 210 μC cm_{Pt}^{-2}. ECA calculations were further validated on polycrystalline Pt, which had a roughness factor of 1.2.

In the cyclic voltammograms, the thickness of the double charging layer on the Pt-Ni nanowires was due to the presence of the graphitized carbon nanofibers. The large capacitance (relative to Pt/HSC) is due to heavy carbon loading (60 wt% on the electrode) relative to Pt (2.9 wt% on the electrode, 7 wt% relative to the mass of Pt and Ni). The coating of electrodes without graphitized carbon nanofibers produced Pt-Ni nanowire cyclic voltammograms similar in shape to polycrystalline Pt.[29] The carbon monoxide oxidation voltammograms and cyclic voltammograms were plotted relative to Pt loading to keep peak heights on a similar scale (data based on electrode area provided in Figure S.1). In terms of electrode-area normalized current, the area by carbon monoxide oxidation is more than an order of magnitude smaller for Pt-Ni nanowires; the calculated ECAs, however, are comparable to Pt/HSC. This was due to the difference in electrode loading on a Pt basis (17.8 μg_{Pt} cm_{elec}^{-2} for Pt/HSC, 2.2 μg_{Pt} cm_{elec}^{-2} for Pt-Ni nanowires).

The peak for carbon monoxide oxidation on Pt-Ni nanowires occurred at a lower potential than Pt/HSC, likely due to Ni at the surface providing oxophilic species in close proximity to Pt sites. The Pt-Ni nanowire carbon monoxide oxidation response also occurred over a larger potential range, likely due to a lack of homogeneity in the mixing of Pt Ni sites at the surface.

ORR activity was determined during anodic linear voltammograms at a scan rate of 20 mV s^{-1} and a rotation speed of 1600 rpm. Activities were taken at 0.9 V vs. RHE and corrected for internal resistance (18–25 Ω), mass transport (Koutecky-Levich equation), and the partial pressure of oxygen (624 mm Hg at 5674 ft). The ORR diffusion-limited currents in this manuscript (4.6–4.9 mA cm_{elec}^{-2}) were lower than commonly observed at sea level due to the lower partial pressure of oxygen at the location where RDE experiments were conducted. These values lie within a theoretically anticipated range by the Levich equation (linearly proportional to the partial pressure of oxygen). Although the diffusion-limited currents were not corrected in ORR polarization curves, the kinetic ORR activities were corrected for the partial pressure of oxygen at a reaction order of 0.75 (previously

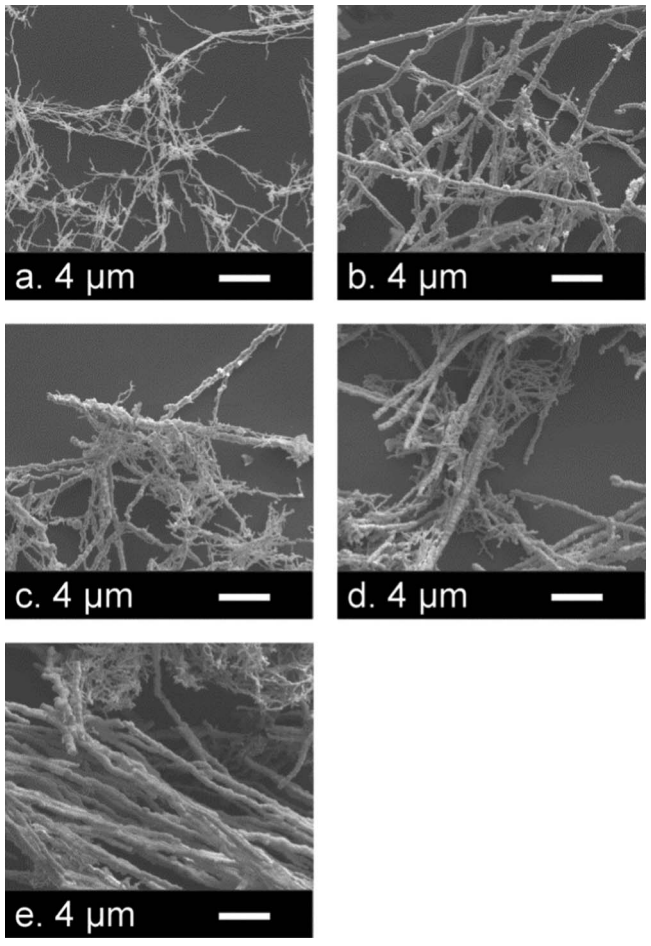

Figure 1. SEM images of Pt-Ni nanowires (7 wt% Pt) (a) untreated and annealed in oxygen to (b) 100, (c) 200, (d) 300, and (e) 500°C following Pt displacement.

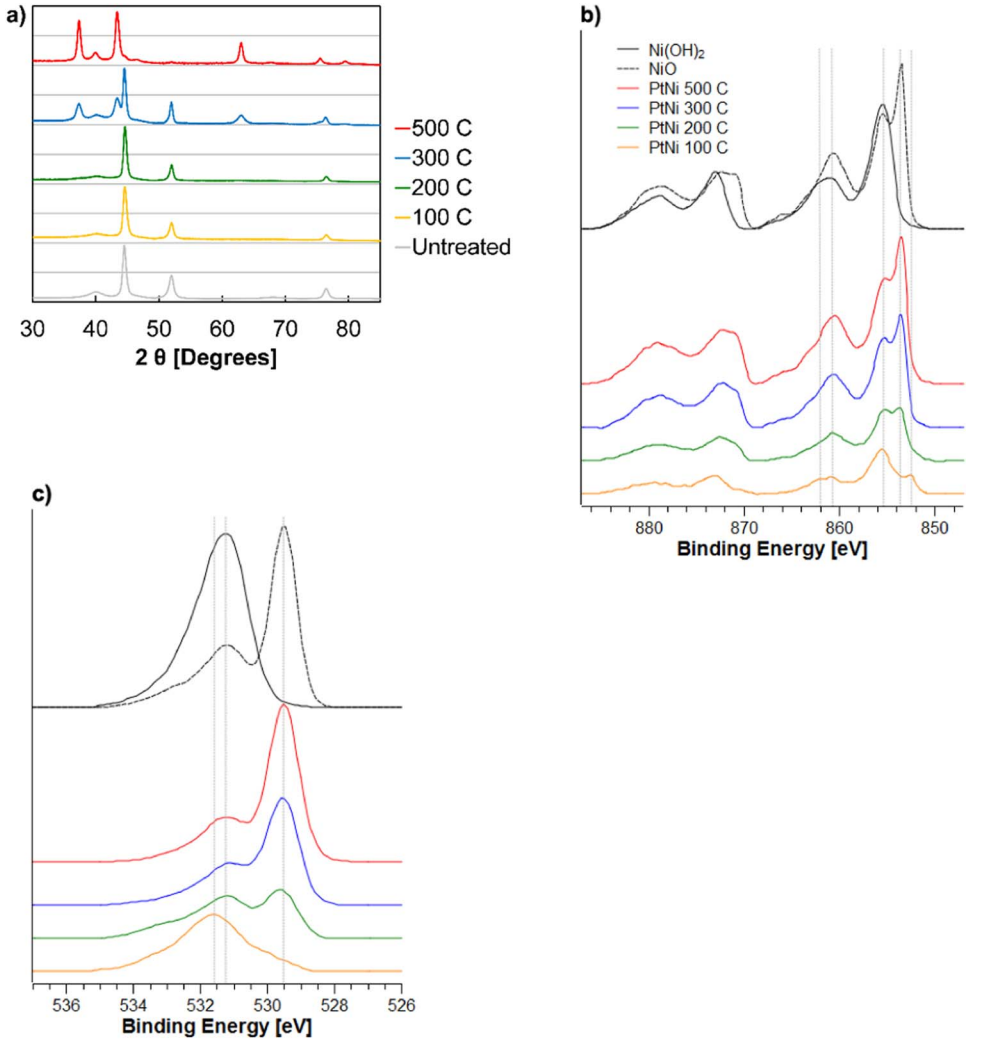

Figure 2. (a) XRD patterns of Pt-Ni nanowires (7 wt% Pt) annealed in oxygen following Pt displacement. High-resolution XPS spectra of Pt-Ni nanowires (7 wt% Pt) annealed in oxygen with reference samples of $Ni(OH)_2$ and NiO (b) Ni 2p and (c) O1s.

determined experimental value at 0.9 V vs. RHE in 0.1 M perchloric acid).[30–32]

Durability experiments were completed in RDE half-cells by performing 30,000 potential cycles (at 500 mV s^{-1}) in the potential range 0.6–1.0 V vs. RHE. Full cyclic voltammograms were taken periodically to monitor fluctuations in ECA. ORR experiments were conducted after durability testing to measure changes in activity. Samples of the electrolyte were also taken following electrochemical break in and durability testing for ICP-MS. Durability experiments were also completed in the potential range 0.0–1.0 V vs. RHE to ensure the stability of Pt-Ni nanowires. Although the Pt-Ni nanowires are durable at lower potentials, complete Pt reduction results in significantly harsher durability conditions for supported or unsupported Pt nanoparticles. This subset of durability data has not been presented here since the potential range is not representative of PEMFC operation, and it would portray an unrealistic durability benefit to using Pt-Ni nanowires.

Results

The annealing temperature used in Pt-Ni nanowire oxidation was found to produce a number of expected trends. As annealing temperature increased, the oxide content increased and wire diameter grew. Through surface sensitive XPS and bulk XRD measurements, this increasing oxide content could be attributed to surface growth followed by bulk NiO formation at high temperatures. These findings are detailed in the following paragraphs in the discussion of Figures 1–3.

As-synthesized Pt-Ni nanowires were 150–250 nm in diameter and 100–200 μm in length (Figure 1). The wire diameter appeared to increase with increasing temperature, and was particularly noticeable at 500°C. Increases in the wire diameter can be attributed to growth by wire shortening and merging, and to the formation (growth) of NiO phase. EDS measurements during SEM experiments showed that the oxygen content increased and the Pt content decreased with increasing temperature (Figure S.2). The comparative increase of oxygen content

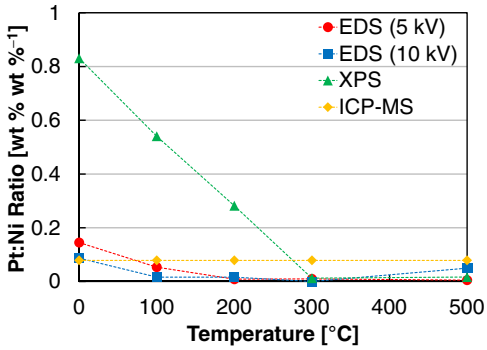

Figure 3. Pt:Ni wt% ratio by EDS, XPS, and ICP of Pt-Ni nanowires annealed in oxygen, with the untreated material included at 0°C.

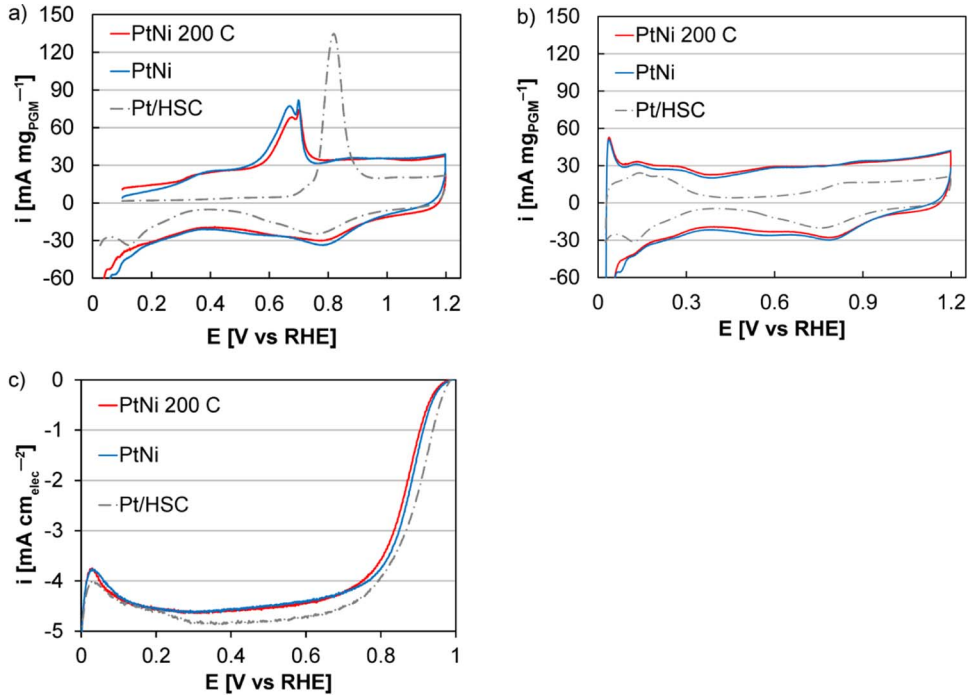

Figure 4. (a) Carbon monoxide oxidation voltammograms, (b) cyclic voltammograms, and (c) ORR polarization curves of Pt-Ni nanowires (untreated and annealed to 200°C) and Pt/HSC at 20 mV s^{-1} in a 0.1 M perchloric acid electrolyte. The ORR diffusion-limited currents observed at 1600 rpm were lower than values expected at sea level, due to the lower partial pressure of oxygen. Further details can be found in the experimental section.

with temperature was likely due to the increased presence of oxide species near the surface and the eventual transition from Ni metal to NiO. XRD patterns also revealed a characteristic Pt lattice of 3.92 Å ((111) peak at 39.8°) in all of the Pt-Ni nanowires (Figure 2). A NiO response began at 300°C ((111) peak at 37.1, (200) peak at 42.9, and (220) peak at 62.4°) and the Ni metal response ((111) peak at 44.5, (200) peak at 51.9, and (220) peak at 76.5°) disappeared completely by 500°C.

XPS further confirmed that as the annealing temperature increased, the oxygen content increased and the Pt content decreased. Nanowires annealed at low temperature showed a high amount of surface carbon species (Figure S.3). From analysis of C 1s and O1s spectra it became apparent that samples annealed at low temperature had high amount of adventitious carbon with a significant concentration of carbon species bonded to oxygen. These species were significantly reduced upon annealing at higher temperatures. Wires treated at lower annealing temperatures showed multiple states of Ni, including metallic Ni (peak at 852.6 eV), hydrous Ni oxide (NiOOH, peak at 855.5 eV), and possibly small amounts of Ni oxide (NiO, 853.5 eV, Figure 2). Increasing the annealing temperature to 200°C led to a decrease in Ni and NiOOH, and an increase in NiO. At 300°C, the Ni 2p and O 1s spectra acquired from nanowires resembled those measured from the NiO reference. The main peak in the Pt 4f spectrum of the Pt-Ni nanowires annealed at 100°C was located at 71.8 eV, a typical location for carbon supported Pt nanoparticles (Figure S.3). In comparison, the spectrum acquired from Pt-Ni nanowires annealed at 200°C is located at 71.5–71.6 eV, indicating a shift closer to the values reported for pure Pt films. XPS confirmed a significant drop in the total amount of surface Pt, occurring after annealing at 300°C (Figures S.3 and S.2b).

Composition of the Pt-Ni nanowires varied depending on the technique, with ICP-MS representing bulk composition and XPS and EDS surface biased composition (Figure 3). As expected, ICP-MS measurements showed no change in the Pt:Ni ratio in any of the samples. XPS and EDS measurements have been normalized in Figure 3 to only include Pt:Ni composition. These measurements are surface sensitive and show an expected increase of Pt content at the surface for non-annealed samples. The trends between the XPS (shortest penetration depth), EDS (5 kV) and EDS (10 kV) (deepest penetration) also show a trend that can be rationalized based on the core shell morphology of these materials for non-annealed samples. Pt:Ni compositions measured by EDS and XPS decreased up to 300°C annealing conditions, exhibiting almost no Pt signal at 300°C. This lack of surface Pt is surprising, and suggests the migration of surface Pt into the nanowire core, results that are consistent with electrochemical results presented later.

The previous figures provide the appropriate background for the electrochemical properties discussed in the rest of the paper. These critical properties are of key importance for the applicability of these materials to oxygen reduction.

Pt-Ni nanowires were characterized for ORR activity in RDE half-cells (Figures 4 and S.4). As the annealing temperature increased, ORR activity decreased and by 250°C, the activity was greatly reduced (Figure 5). Low temperature annealing (to 150°C) did not impact catalyst durability, and large mass activity losses were observed with

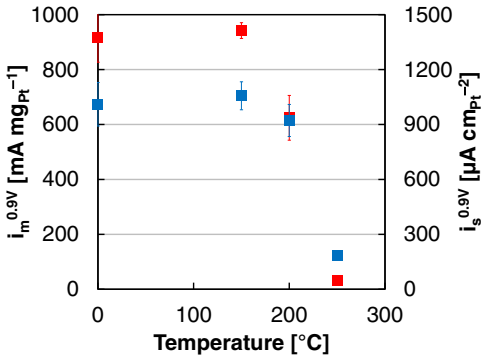

Figure 5. Mass and specific ORR activities of Pt-Ni nanowires as a function of annealing temperature, with the untreated Pt-Ni nanowires included at 0°C. ORR activities were determined during anodic polarization scans at 1600 rpm and 20 mV s^{-1} in oxygen-saturated 0.1 M perchloric acid.

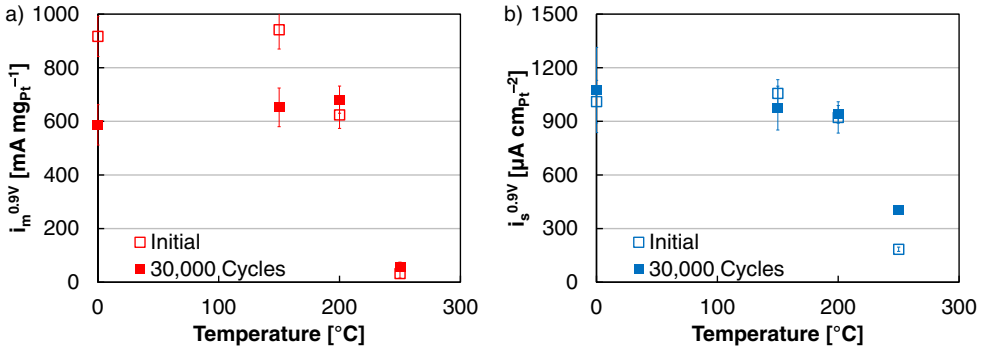

Figure 6. (a) Mass and (b) specific ORR activities of Pt-Ni nanowires, prior to and following durability, as a function of annealing temperature. Activities of the untreated Pt-Ni nanowires were included at 0°C. ORR activities were determined during anodic polarization scans at 1600 rpm and 20 mV s^{-1} in oxygen-saturated 0.1 M perchloric acid. Durability testing was completed by potential cycling (0.6–1.0 V vs. RHE) 30,000 times in a RDE half-cell.

both the as-synthesized Pt-Ni nanowires and the material annealed to 150°C. An improvement in durability was found for the nanowires annealed to 200°C, which had the highest ORR mass activity performance following potential cycling (Figures 6, S.4, and S.5). This study was repeated for Pt-Ni nanowires at a variety of Pt contents (3.4, 12.1, 16.7, and 95.4 wt% Pt). On occasion, these iterations were comparable to 7.3 wt% Pt in terms of oxygen reduction durability and Ni dissolution on a percentage basis (Figures S.6 and S.7). Since the activities of the materials were lower, however, they were of less interest.

Annealing of the Pt-Ni nanowires produced desired trends in Ni dissolution, as increasing the annealing temperature increased oxide formation and slowed Ni dissolution (Figure 7). All samples showed some Ni dissolution upon exposure to acid and additional dissolution during potential cyclying. At higher annealing temperature, Ni release was greatly reduced but still resulted in a meaningful and potentially significant dissolution rate. Ni dissolution was not an issue in the electrochemical performance of the RDE tests performed, but is critical for the performance of these materials in MEAs. We have investigated these and related materials in fuel cells and found that Ni contamination is a pressing concern.[33] The improvement in dissolution rate observed is meaningful, but dissolution rates observed are believed to be still too high for most applications, for the high initial Ni content catalysts explored here.

Ni^{2+} is thermodynamically favorable under acidic conditions at the potentials of interest whether starting as nickel metal or nickel oxide (NiO). Ni metal doesn't dissolve as Ni metal, but reacts from Ni to Ni^{2+}, either forming a Ni oxide first or just dissolving into solution.

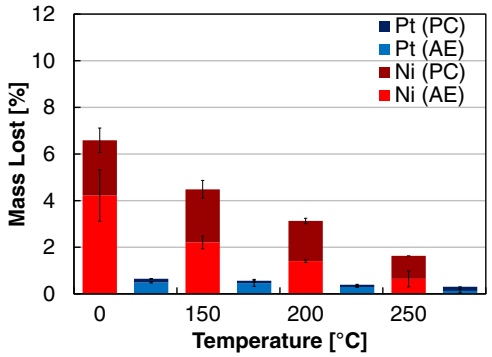

Figure 7. Total catalyst mass (Ni and Pt) lost intro the liquid electrolyte following acid exposure (electrochemical break in, denoted AE) and potential cycling (durability testing, denoted PC). Percentages were determined by ICP-MS and data was presented as a function of annealing temperature. Durability testing was completed by potential cycling (0.6–1.0 V vs. RHE) 30,000 times in a RDE half-cell. Percentages were plotted relative to the total catalyst mass.

The observed dissolution rates are controlled by kinetics, and contain both the reaction and dissolution of nickel metal.[34] At increased annealing temperature, Ni metal near the surface is oxidized, increasing the thickness of the oxide layer. The exact kinetics or mechanism of this process is unclear, but ICP-MS data clearly demonstrates that Ni dissolution during electrochemical testing slows with increasing oxidative treatments (Figures 7 and S.7). The decreased dissolution rates could be due to an increased dissolution potential when oxide layers aren't present, or the impact of thick oxide layers in slowing the process, perhaps due electron transport as a critical step in the process and the decreased conductivity of the oxide layer. Previous studies have on occasion found that the formation of Ni oxide layers can passivate or slow the electrochemical dissolution of Ni in acidic electrolytes.[35,36] This examination also leverages findings from two previous publications, where Pt displacement as an acidic cation preferentially displaces Ni metal instead of Ni oxides, and oxidative treatments reduce Ni dissolution in Pt-Ni nanowires during electrochemical characterization for the methanol oxidation reaction in RDE half-cells.[1,37] Ni nanowires, as-received and annealed in oxygen, were also exposed to acids at a variety of concentrations (Figure S.8). Increasing the annealing temperature and the Ni oxide layer thickness slowed the process of Ni dissolution in all cases examined. Although these results do not include Pt or an applied potential, they do definitively conclude that the dissolution of NiO is slower than Ni metal in dilute acid and they parallel the results presented throughout this paper.

Conclusions

Pt-Ni nanowires were annealed in oxygen in an effort to improve durability and minimize Ni dissolution. Pt-Ni nanowires demonstrate exceptional activity for ORR, particularly at low levels of galvanic displacement where the noble layer can be thrifted, improving Pt utilization and ECA. The displacement of extended surface catalysts has shown promise, taking advantage of the high site-specific activity of extended surfaces while exceeding the ECAs typically produced by other deposition techniques.

The data in this paper is largely summarized in Table I to allow comparisons to be made more easily between samples and measured properties. Annealing Pt-Ni nanowires in oxygen yielded a tradeoff of initial activity for durability (Table I). With increased annealing temperature, the activity and ECA decreased at temperatures greater than 150°C. Following durability testing however, the retention of activity improved with increased temperature. While the untreated and 150°C materials lost 37% and 31% of their initial mass activity, the 200°C and 250°C catalysts gained 9% and 88%.

For the Pt-Ni nanowires annealed to 200°C, their initial activity was less (32%) than the as-synthesized material. Following potential cycling, however, their activity (9%) and ECA (2%) improved, eliminating the losses of the untreated catalyst. The mass activity after

Table I. ORR mass activities (i_m), specific activities (i_s), ECAs, and Ni dissolution rates (following acid exposure, denoted Ni_{AE} and after durability by potential cycling, denoted Ni_{PC}) prior to and following durability testing. Ni dissolution listed relative to the total catalyst mass.

	$i_{m,i}$ [mA mg_{Pt}^{-1}]	$i_{m,f}$ [mA mg_{Pt}^{-1}]	$i_{s,i}$ [μA cm_{Pt}^{-2}]	$i_{s,f}$ [μA cm_{Pt}^{-2}]	ECA_i [m^2 g_{Pt}^{-1}]	ECA_f [m^2 g_{Pt}^{-1}]	Ni_{AE} [%]	Ni_{PC} [%]
Untreated	917	582	1011	1075	91	54	4.2	2.4
150°C	942	653	1057	974	89	67	2.2	2.3
200°C	624	680	922	939	68	72	1.4	1.7
250°C	30	57	184	406	16	14	0.6	1.0
Pt/HSC	310	225	304	278	102	81	–	–

durability (680 mA mg_{Pt}^{-1}) was the highest observed, 3 times greater than Pt/HSC and 1.5 times greater than the DOE-MEA target. Ni dissolution rates were also reduced at elevated temperature, from 7.2% for the as-synthesized nanowires to 3.4% at 200°C.

The focus of this study has been on catalysts with 7 wt% Pt, since these materials have previously demonstrated a maximum in ECA and ORR activity. The high Ni content, however, increases the concern for Ni dissolution. These findings may not be as important for other systems with different structures or lower Ni content. We focused on Pt-Ni nanowires due to their high performance relative to others materials that we have explored, and found that NiO layer growth offers improvements in durability. These materials are still subject to dissolution at a rate that likely prevents it from becoming a viable solution by itself. While Ni dissolution is potentially less of a concern at high Pt content, annealing in oxygen may improve the stability of ORR catalysts with different structures and electrochemical catalysts where metal dissolution is a concern.

Acknowledgments

The authors thank and acknowledge the contributions of Clay Macomber, who developed the ICP-MS parameters and methodology and Justin Bult, who annealed preliminary materials in this study.

Financial support is provided by the U.S. Department of Energy, Office of Energy Efficiency and Renewable Energy, through contract no. DE-AC36-08GO28308 to the National Renewable Energy Laboratory.

References

1. S. M. Alia, B. A. Larsen, S. Pylypenko, D. A. Cullen, D. R. Diercks, K. C. Neyerlin, S. S. Kocha, and B. S. Pivovar, *ACS Catalysis*, **4**, 1114 (2014).
2. R. Borup, J. Meyers, B. Pivovar, Y. Kim, R. Mukundan, N. Garland, D. Myers, M. Wilson, F. Garzon, D. Wood, P. Zelenay, K. More, K. Stroh, T. Zawodzinski, J. Boncella, J. McGrath, M. Inaba, K. Miyatake, M. Hori, K. Ota, Z. Ogumi, S. Miyata, A. Nishikata, Z. Siroma, Y. Uchimoto, K. Yasuda, K. Kimijima, and N. Iwashita, *Chemical Reviews*, **107**, 3904 (2007).
3. P. Ferreira, G. la O', Y. Shao-Horn, D. Morgan, R. Makharia, S. Kocha, and H. Gasteiger, *Journal of the Electrochemical Society*, **152**, A2256 (2005).
4. H. Gasteiger, S. Kocha, B. Sompalli, and F. Wagner, *Applied Catalysis B: Environmental*, **56**, 9 (2005).
5. V. Stamenkovic, B. Mun, K. Mayrhofer, P. Ross, N. Markovic, J. Rossmeisl, J. Greeley, and J. Nørskov, *Angew. Chem.*, **118**, 2963 (2006).
6. V. Stamenković, T. Schmidt, P. Ross, and N. Marković, *J. Phys. Chem. B*, **106**, 11970 (2002).
7. U. Paulus, A. Wokaun, G. Scherer, T. Schmidt, V. Stamenkovic, N. Markovic, and P. Ross, *Electrochim. Acta*, **47**, 3787 (2002).
8. V. Stamenkovic, B. Fowler, B. Mun, G. Wang, P. Ross, C. Lucas, and N. Marković, *Science*, **315**, 493 (2007).
9. C. Cui, L. Gan, H. Li, S. Yu, M. Heggen, and P. Strasser, *Nano Letters*, **12**, 5885 (2012).
10. C. Cui, L. Gan, M. Heggen, S. Rudi, and P. Strasser, *Nat Mater*, **12**, 765 (2013).
11. U. A. Paulus, A. Wokaun, G. G. Scherer, T. J. Schmidt, V. Stamenkovic, N. M. Markovic, and P. N. Ross, *Electrochimica Acta*, **47**, 3787 (2002).
12. U. Paulus, A. Wokaun, G. Scherer, T. Schmidt, V. Stamenkovic, V. Radmilovic, N. Markovic, and P. Ross, *The Journal of Physical Chemistry B*, **106**, 4181 (2002).
13. S. Du, Y. Lu, S. Malladi, Q. Xu, and R. Steinberger-Wilckens, *Journal of Materials Chemistry A*, **2**, 692 (2014).
14. K. Gong, D. Su, and R. R. Adzic, *Journal of the American Chemical Society*, **132**, 14364 (2010).
15. K. A. Kuttiyiel, K. Sasaki, Y. Choi, D. Su, P. Liu, and R. R. Adzic, *Nano Letters*, **12**, 6266 (2012).
16. X. Huang, Z. Zhao, L. Cao, Y. Chen, E. Zhu, Z. Lin, M. Li, A. Yan, A. Zettl, Y. M. Wang, X. Duan, T. Mueller, and Y. Huang, *Science*, **348**, 1230 (2015).
17. V. Stamenković and N. Marković, Nanosegregated Cathode Catalysts with Ultra-Low Platinum Loading, in, U. S. Department of Energy Editor, http://www.hydrogen.energy.gov/pdfs/review14/fc008_stamenkovic_2014_o.pdf (2014).
18. C. Chen, Y. Kang, Z. Huo, Z. Zhu, W. Huang, H. L. Xin, J. D. Snyder, D. Li, J. A. Herron, M. Mavrikakis, M. Chi, K. L. More, Y. Li, N. M. Markovic, G. A. Somorjai, P. Yang, and V. R. Stamenkovic, *Science*, **343**, 1339 (2014).
19. D. van der Vliet, C. Wang, M. Debe, R. Atanasoski, N. Markovic, and V. Stamenkovic, *Electrochimica Acta*, **56**, 8695 (2011).
20. M. Debe in U. S. Department of Energy Editor, http://www.hydrogen.energy.gov/pdfs/review09/fc_17_debe.pdf (2009).
21. Z. Chen, M. Waje, W. Li, and Y. Yan, *Angewandte Chemie International Edition*, **46**, 4060 (2007).
22. S. Alia, G. Zhang, D. Kisailus, D. Li, S. Gu, K. Jensen, and Y. Yan, *Advanced Functional Materials*, **20**, 3742 (2010).
23. B. Larsen, K. Neyerlin, J. Bult, C. Bochert, J. Blackburn, S. Kocha, and B. Pivovar, *Journal of the Electrochemical Society*, **159**, F622 (2012).
24. S. Alia, K. Jensen, B. Pivovar, and Y. Yan, *ACS Catalysis*, **2**, 858 (2012).
25. S. Alia, K. Jensen, C. Contreras, F. Garzon, B. Pivovar, and Y. Yan, *ACS Catalysis*, **3**, 358 (2013).
26. S. M. Alia, S. Pylypenko, K. C. Neyerlin, D. A. Cullen, S. S. Kocha, and B. S. Pivovar, *ACS Catalysis*, **4**, 2680 (2014).
27. S. M. Alia, Y. Yan, and B. Pivovar, *Catalysis Science & Technology*, **4**, 3589 (2014).
28. K. C. Neyerlin, B. A. Larsen, S. Pylypenko, S. S. Kocha, and B. S. Pivovar, *ECS Transactions*, **50**, 1405 (2013).
29. S. M. Alia, Y. S. Yan, and B. S. Pivovar, *Catalysis Science & Technology*, **4**, 3589 (2014).
30. K. C. Neyerlin, W. Gu, J. Jorne, and H. A. Gasteiger, *Journal of the Electrochemical Society*, **153**, A1955 (2006).
31. I. Takahashi and S. S. Kocha, *Journal of Power Sources*, **195**, 6312 (2010).
32. S. S. Kocha, in *Handbook of Fuel Cells – Fundamentals, Technology and Applications*, W. Vielstich, A. Lamm, and H. A. Gasteiger Editors, p. 538 (2003).
33. B. Pivovar, Extended, Continuous Pt Nanostructures in Thick, Dispersed Electrodes, in, U.S. Department of Energy Editor, http://www.hydrogen.energy.gov/pdfs/review14/fc007_pivovar_2014_o.pdf (2014).
34. J. W. Schultze and M. Lohrengel, *Electrochimica Acta*, **45**, 2499 (2000).
35. M. Barbosa, S. Real, J. Vilche, and A. Arvia, *Journal of The Electrochemical Society*, **135**, 1077 (1988).
36. J. Scherer, B. Ocko, and O. Magnussen, *Electrochimica Acta*, **48**, 1169 (2003).
37. S. M. Alia, S. Pylypenko, K. Neyerlin, S. S. Kocha, and B. S. Pivovar, *ECS Transactions*, **64**, 89 (2014).